SCIENCE CHINA
Earth Sciences

• RESEARCH PAPER •

doi: 10.1007/s11430-016-0101-6

Lateral variation in seismic velocities and rheology beneath the Qinling-Dabie orogen

DENG YangFan[1*], CHEN Lin[2], XU Tao[2,3], WU Jing[2], Fabio ROMANELLI[4] & Giuliano Francesco PANZA[4,5,6]

[1] *State Key Laboratory of Isotope Geochemistry, Guangzhou Institute of Geochemistry, Chinese Academy of Sciences, Guangzhou 510640, China;*
[2] *State Key Laboratory of Lithospheric Evolution, Institute of Geology and Geophysics, Chinese Academy of Sciences, Beijing 100029, China;*
[3] *Chinese Academy of Sciences Center for Excellence in Tibetan Plateau Earth Sciences, Beijing 100101, China;*
[4] *Department of Mathematics and Geosciences, University of Trieste, Via Weiss, I-34127 Trieste, Italy;*
[5] *Institute of Geophysics, China Earthquake Administration, Beijing 100081, China;*
[6] *ISSO-International Seismic Safety Organization, Viale San Francesco, 12, I-64031 Arsita, Italy*

Received July 10, 2016; accepted November 1, 2016; published online January 16, 2017

Abstract The Qinling-Dabie orogen is an important tectonic belt that trends east-west and divides continental China into northern and southern parts. Due to its strong deformation, complicated structure, multiphase structural superposition and the massive exposed high and ultrahigh metamorphic rocks, its tectonic formation and geodynamical evolution are hot research topics worldwide. Previous studies mainly focused on the regional geological or geochemical aspects, whereas the geophysical constraints are few and isolated, in particular on the orogenic scale. Here, we integrate the available P- and S-wave seismic and seismicity data, and construct the rheological structures along the Qinling-Dabie orogen. The results demonstrate that: (1) there are strong lateral variations in the crustal velocity between the western and eastern sections of the Qinling-Dabie orogen, indicating the different origin and tectonic evolution between these two parts; (2) the lateral variations are also manifested in the rheological structure. The rigid blocks, such as South China and Ordos basin (North China Craton), resist deformation and show low seismicity. The weak regions, such as the margin of Tibet and western Qinling-Dabie experience strong deformation and accumulated stress, thus show active seismicity; (3) in the lower crust of most of the HP/UHP terranes the values of P-wave velocity are higher than the global average ones; finally (4) low P- and S-wave velocities and low strength in the lower crust and lithospheric mantle beneath Dabie indicate lithospheric delamination, and/or high temperature, and partial melting condition.

Keywords Qinling-Dabie orogen, Deep seismic sounding, Tomography, Rheology, Seismicity

Citation: Deng Y F, Chen L, Xu T, Wu J, Romanelli F, Panza G F. 2017. Lateral variation in seismic velocities and rheology beneath the Qinling-Dabie orogen. Science China Earth Sciences, 59: 1–13, doi: 10.1007/s11430-016-0101-6

1. Introduction

The East-West trending Qinling-Dabie orogen is situated between the southern margin of the North China Craton and the northern margin of the Yangtze block (Figure 1). Since the middle of 1980s, when coesite and microdiamonds were found as inclusions in minerals from eclogites and surrounding gneisses in the Dabie orogen (eastern-central China), deep continental subduction, high and ultrahigh pressure (HP/UHP), metamorphism, and subsequent exhumation in the Qinling-Dabie orogen have become hot issues in this region (e.g. Liou et al., 2000; Zheng, 2008; Xu et al., 2014; Dong et al., 2011; Zheng et al., 2012).

Previous studies have mainly emphasized the geochemical and geological aspects (Meng and Zhang, 2000; Zhang et al.,

*Corresponding author (email: yangfandeng@gig.ac.cn)

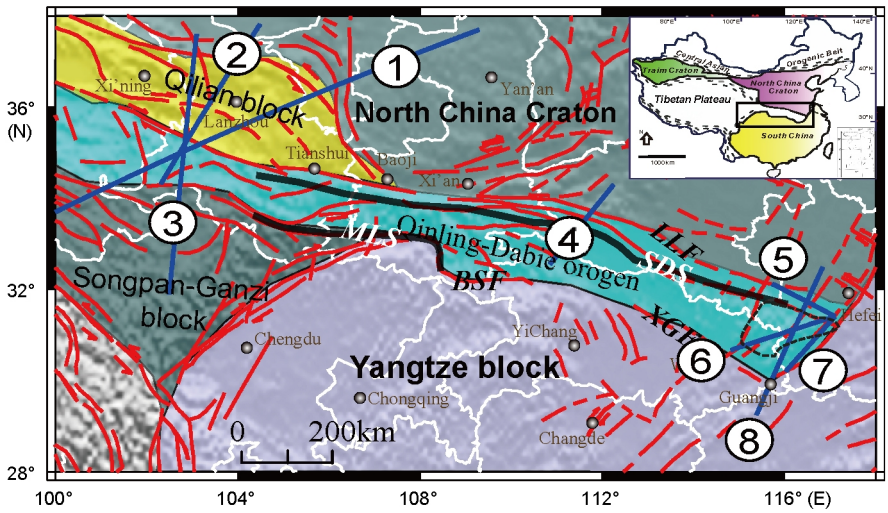

Figure 1 DSS profiles conducted in the Qinling-Dabie orogen. The inset map in the top-right corner shows the study region in China mainland. The tectonic units are from Dong et al. (2011). The red lines indicate faults; the white lines indicate the province boundaries; the dashed black line indicates the Dabie dome. LLF, Luonan-Luanchuan fault; BSF, Bashan fault; XGF, Xiangfan-Guangji fault; SDS, Shangdan suture zone; MLS, Mianlue suture zone. The circled numbers outline the profiles: 1, Maqin-Jianbian (Liu et al., 2006); 2, Hezuo-Jingtai (Zhang et al., 2013a); 3, Maerkang-Gulang (Zhang et al., 2008); 4, Yichuan-Shiyan (Cao et al., 1994); 5, Gushi-Lujiang (Liu et al., 2003); 6, Tuanfeng-Lujiang (Liu et al., 2003); 7, Huangmei-Lujiang (Liu et al., 2003); 8, Zhangmu-Anyi (Dong et al., 1998).

2003, 2004; Zheng et al., 2007; Zheng, 2008). Detailed physical features at certain depth remain unclear, even if several seismic profiles conducted unconnectedly in this region (Cao et al., 1994; Dong et al., 1998; Liu et al., 2003, 2006; Zhang et al., 2008, 2013a) traverse the Qinling-Dabie orogen and reveal some details of the 2D crustal structure of the orogen. Benefitting from these abundant geophysical data, it is desirable to give a comprehensive and regional analysis on this complex region.

In this study, we focus on the Qinling-Dabie orogen by analysing the existing P-wave velocity (*Vp*) and S-wave velocity (*Vs*) models and constructing lithospheric rheology profiles in order to study the lithospheric characteristics. In terms of the widely distributed HP/UHP rocks in this region, it is of great significance to compare the major features of the lithosphere in the study area with those of other UHP terranes worldwide.

2. P-wave velocity beneath the Qinling-Dabie orogen and neighbouring region

2.1 Dataset

In order to understand the crustal feature beneath the Qinling-Dabie orogen a 280-km-long wide-angle seismic profile (Deep seismic sounding, DSS) named Yichuan-Shiyan profile (Cao et al., 1994), and a 420-km-long profile, named Zhuangmu-Anyi profile (Dong et al., 1998) were performed by the Chinese Academy of Geological Sciences in the eastern and central Qinling-Dabie orogen (profiles labelled 4, 8 in Figure 1). With the purpose of studying the fine structure beneath this continental subduction zone, the project "Continental deep subduction" was accomplished in 2001 and the *Vp* along the Gushi-Lujiang, Tuanfeng-Lujiang and Huangmei-Lujiang profiles (labelled 5–7 in Figure 1) were obtained from high resolution seismic travel time tomography (Liu et al., 2003). The China Earthquake Administration (CEA) took over the 1000-km-long Maqin-Jingbian DSS profile (labelled 1 in Figure 1) in north-eastern Tibet in 1997 (Liu et al., 2006), and in 2004 the Markang-Gulang profile (labelled 3 in Figure 1) was conducted in order to understand the uplift mechanism of Tibet and the coupling interaction between basin and orogen (Zhang et al., 2008). More recently, our group conducted the 637-km-long Hezuo-Jingtai profile to study the crustal difference among the Qilian and Qinling Dabie orogens, and the Tibetan Plateau (Zhang et al., 2013a) (labelled 2 in Figure 1).

As shown in Figure 1, the DSS profiles span across the Qinling-Dabie orogen, the North China Craton, the Yangtze block, the Qilian block and the Songpan-Ganzi block. Thus, we can compare the seismic velocity features among these blocks, with special attention to the differences between the eastern and western parts, on one side, and between the northern and southern parts, on the other.

2.2 Differences between western and eastern parts

Figure 2 displays the interpretations of the seismic dataset and the crustal velocity models along the 8 DSS profiles. Concentrated within the interior of the Qinling-Dabie orogen, there are remarkable differences between the eastern and western

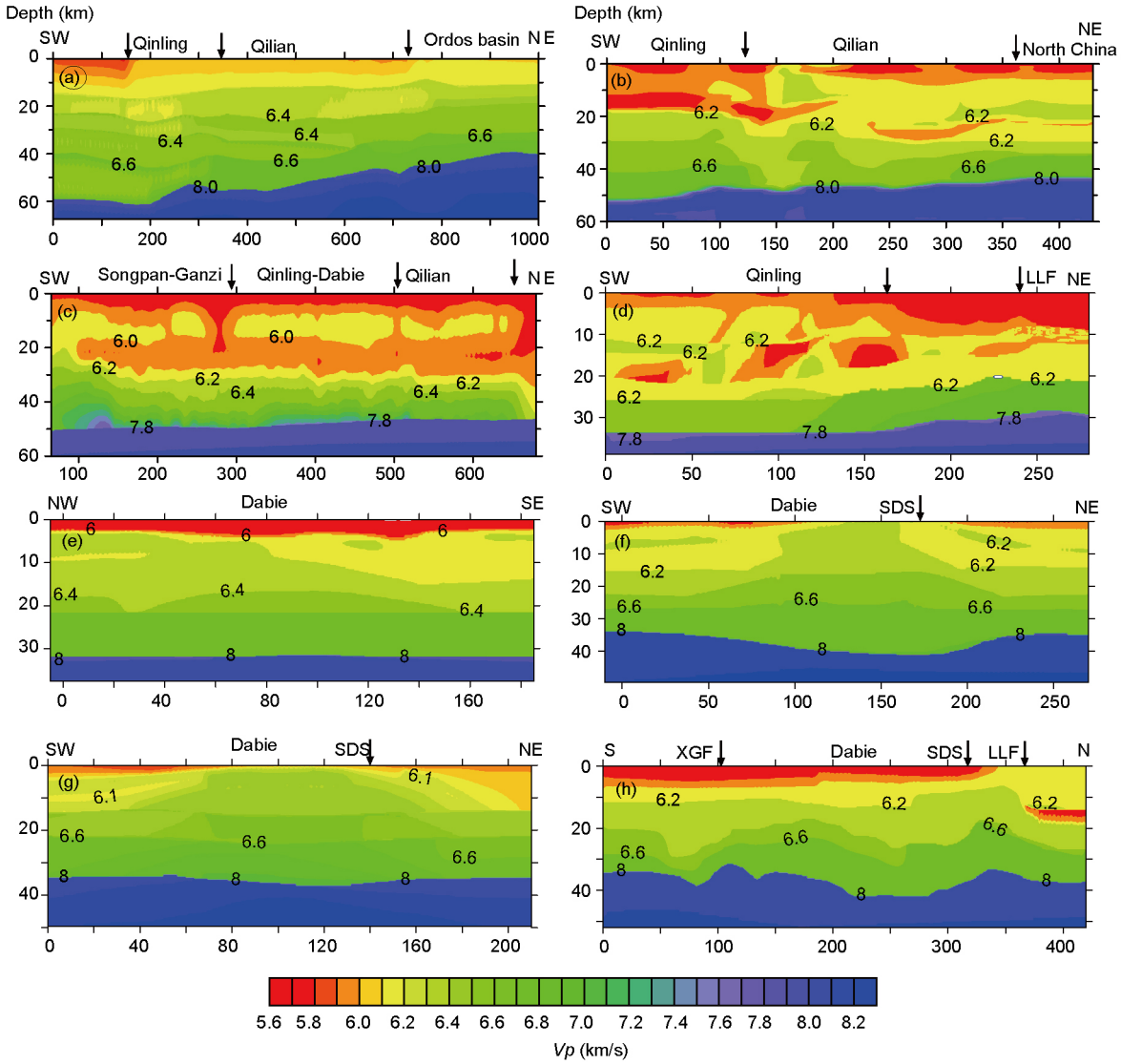

Figure 2 Crustal P-wave velocity models, corresponding to the eight DSS profiles presented in Figure 1. The tectonic units are the same as in Figure 1. (a) Profile 1; (b) profile 2; (c) profile 3; (d) profile 4; (e) profile 5; (f) profile 6; (g) profile 7; (h) profile 8.

parts. For instance, the Moho depth reaches ~50 km in the western Qinling-Dabie and rises to ~35 km in the central Qinling-Dabie. The low velocity layer in the upper or middle crust is a common feature in the west profiles.

In the crust of the eastern Qinling-Dabie orogen there is a high-velocity dome (Dabie complex) and the velocity in the shallower part (< 5 km) beneath the core of the dome reaches 6.0 km/s, indicating metamorphic rocks of the middle- and lower-crusts exposed at the surface. On both sides of the dome, a low velocity layer (body) with ~6.1 km/s is present in upper-middle crust. The Moho depth reaches the peak (~41 km) at the core, compared with 32–34 km at both sides of the orogen; a 4 km Moho-offset is observed beneath the Xiaotian-Mozitan Fault (beside SDS). Liu et al. (2003) recognize that the velocity-pattern in the eastern Dabie orogen is typical for continent-continent deep subduction/collision. The Moho offset may be related with the suture zone of the Yangtze and North China Craton collision. Therefore, the high-velocity dome indicates the product of the collision/extrusion between the continental blocks (Liu et al., 2003), or the cooling and crystallization of intrusive igneous rocks in the middle crust resulting from the post-collisional lithosphere delamination and subsequent magmatism (Luo et al., 2012).

Figure 3 presents the average *Vp* along the profiles. The *Vp* changes gently from west to east along profile 1, namely ~6.3 km/s in Qinling, ~6.35 km/s in the Qilian block, ~6.4 km/s in the Ordos basin (North China Craton), consistently with the result of passive seismic experiment (Pan and Niu, 2011). Along profile 3, the velocity is fairly stable in the Songpan-Ganzi, Qinling-Dabie, and Qilian block (~6.2 km/s). Another interesting feature is that the average velocity in the western and central profiles is lower (less than 6.4 km/s) than the one in the eastern profiles. This feature implies a more felsic composition of crust or a higher temperature in the western part

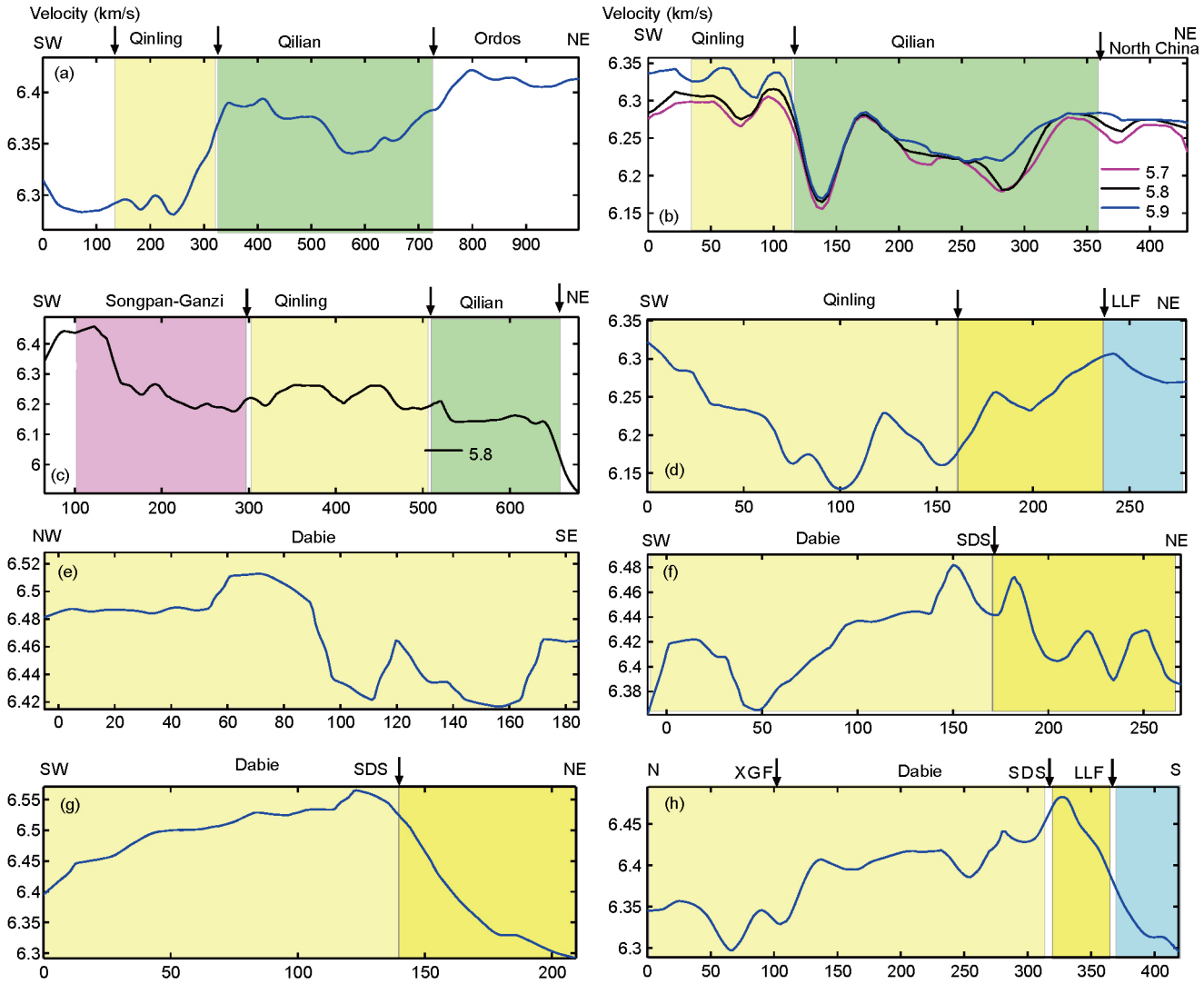

Figure 3 Average P-wave velocities (km/s) of crystalline crust (removing the sedimentary effect). The tectonic units are the same as in Figure 1. (a) Profile 1; (b) profile 2; (c) profile 3; (d) profile 4; (e) profile 5; (f) profile 6; (g) profile 7; (h) profile 8.

with respect to the eastern one (e.g., Rudnick and Fountain, 1995).

2.3 Differences between northern and southern parts

The Moho depth rises gradually from south to north as shown in profiles 1–4 (Figure 2). Specifically, along profile 1 the Moho depth is ~60 km in the Songpan-Ganzi block, rising abruptly to ~52 km in the Qinling block. Whereas in the north, beneath the Ordos basin, the Moho depth is ~42 km. Along profile 2 the Moho depth is ~50 km beneath the Qinling block and rises gradually to 43 km beneath the North China Craton. Along profiles 3 and 4, the Moho depth undulates from ~51 to 46 km and from ~33 to 29 km, respectively. The Moho depth is relatively flat beneath profile 5. By contrast, along profiles 6–8, it is deeper than 40 km beneath the core of Dabie. According to profile 8 and a deep seismic reflection profile, two zones with (distinct) overlapping Moho have been identified by Dong et al. (2008). It was argued that structural remnants of the Triassic deep continental subduction remained preserved, despite the superimposed Jurassic deformation. From the receiver function studies, the imaged high-velocity volumes in the mantle beneath the southern NCC were interpreted as a subduction remnant, which reveals a flat subduction channel resulted from the continent-continent collision between the NCC and the Yangtze craton (Zheng et al., 2012).

3. S-wave velocity structure of the lithosphere-asthenosphere system

Using data from more than 2000 seismic stations from multiple networks arrayed throughout China (CEArray, China Array, NECESS, PASSCAL, GSN) and surrounding regions (Korean Seismic Network, F-Net, KNET), Shen et al. (2016)

performed ambient noise Rayleigh wave tomography across the China mainland. The isotropic Rayleigh wave group and phase speed maps from 8 to 50 s are obtained from ambient noise tomography, and then, by including earthquake surface wave data, the period range has been extended to 70 s. A Monte-Carlo inversion method (Shen et al., 2013) is employed to estimate a 3-D V_{SV} model of the crust and uppermost mantle. Compared with the previous surface wave tomography studies in this region (Zhou et al., 2012; Xie et al., 2013; Zhang Z et al., 2014; Zhang X M et al., 2014; Jiang et al., 2016), this model has a better resolution due to its denser coverage and longer duration of recording time. Consequently, we select this cellular model (0.5°×0.5°) as representative of our study area (Figure 4).

To the east of the study region (east of 111°E) the cells (or columns) have a relatively thin crust (lower than 40 km), except for cell G05, lying beneath the Dabie orogen. To the west, the Moho depth increases gradually, reaching a thick-

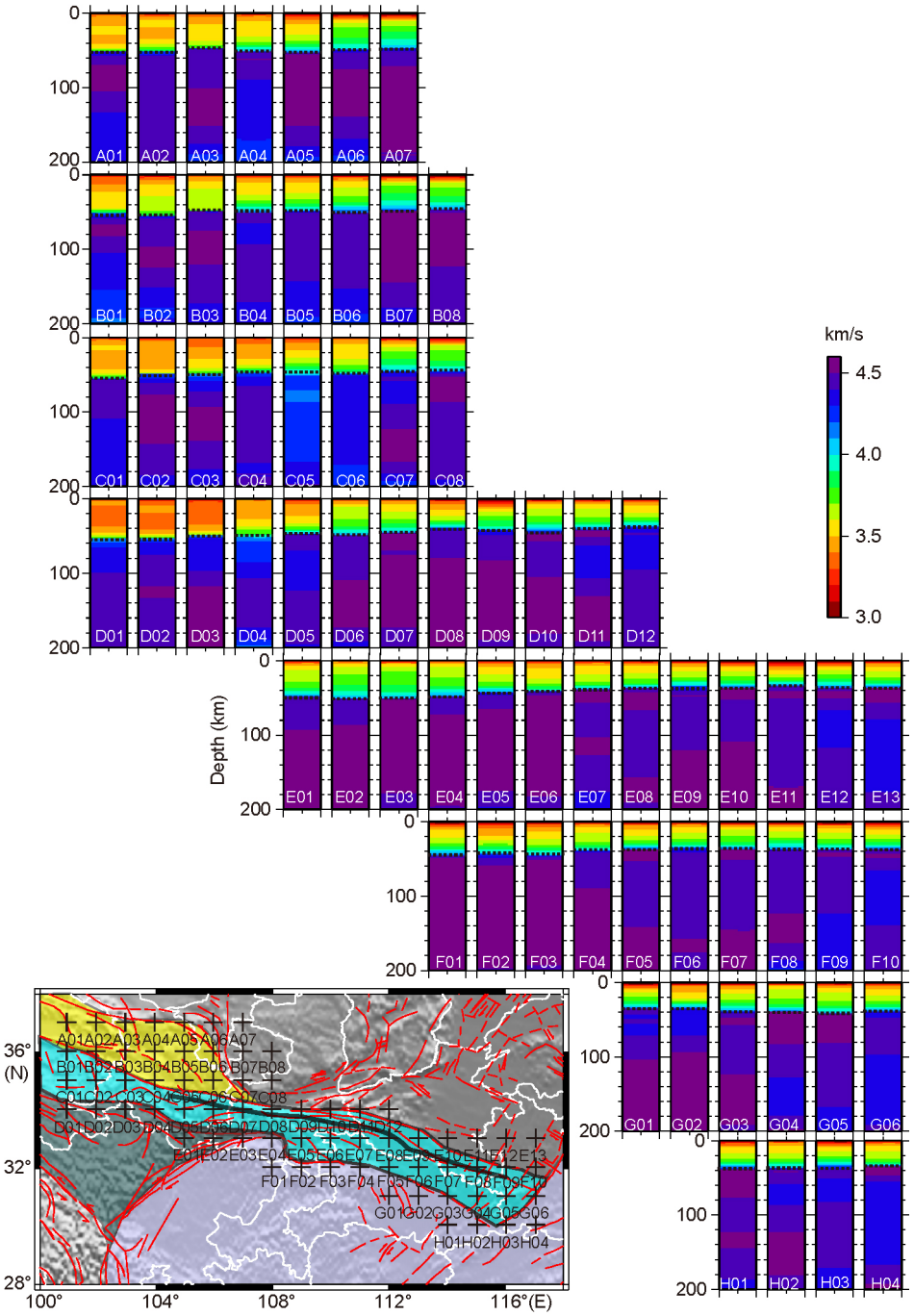

Figure 4 S-wave velocities (km/s) of the lithosphere-asthenosphere system beneath the Qinling-Dabie orogen and its adjacent areas (Shen et al., 2016). Black dashed lines represent the Moho depth.

ness larger than 55 km in cells A01, A02, B01, B02, C01, C02, D01, and D02. In cells B08, C08, E10, E11, E12 and E13, the low velocity in the shallow part reveals the sedimentary basin features in the North China Craton. Another interesting feature is that the low velocity is common in the crust in the western part (A01, A02, B01, B02, C01, C02, C03, D01, D02, D03), which is consistent, to some extent, with the DSS results. The North China and Yangtze cratons (cells A06, A07, B07, B08, C08, D09, D10, E03, E04, E05, E06, E12, F01, F02, F03, G01, G02, H01) are well known to be in a stable tectonic condition with a rigid lithosphere (Deng et al., 2011; Zhang et al., 2013b), showing lithospheric mantle *Vs* higher than 4.5 km/s. However, beneath the Dabie orogen (cells F08, F09, G04, G05, G06, H03) mantle *Vs* is not very high ($\leq$ 4.5 km/s), indicating a possible higher temperature in the mantle lithosphere reaching a partial melting condition, if compared to the Yangtze block (cells E02, E03, E04, E05, F01, F02, F03) and the North China Craton (cells B07, B08, C07, C08, D11, D12, E10, E11) (e.g. see Ouyang et al., 2014; Vanderhaeghe and Teyssier, 2001). The velocity is consistent with other geophysical observations (e.g. Wang et al., 2005, 2007; Zheng et al., 2011; Bao et al., 2013; Jiang et al., 2013) and the lithospheric thinning/delamination proposed by geochemical studies (Gao et al., 1999; Zhang et al., 2015). On account of the common low velocities in the eastern part (cells E12, E13, F9, F10, G05, G06, H03,H04), the possible effect of the Paleo-Pacific plate subduction (Ouyang et al., 2014; Zheng et al., 2014) represents another reasonable interpretation.

One alternative reason for the difference of P-wave and S-wave velocities between western and eastern parts is their original history: the western segment is an accretionary-type arc-continent collisional orogen, whereas the eastern segment is a simple continent-continent collisional orogen (Wu and Zheng, 2013; Zhang et al., 2013a). On the other hand, the Cenozoic activities in the western part (Indian-Asian collision) produce the continuous crustal shortening and shear heating (Chen and Gerya, 2016), which leads to a thicker crust but lower crustal velocity.

4. Rheological differences among the blocks

Velocity is an important physical feature of the geodynamic processes (present or past), while rheology controls the deformation. The geodynamic processes can be evaluated by considering the flux of material in the deep crust, which could be inferred from the rheological structure of the lithosphere (e.g. Panza and Raykova, 2008; Brandmayr et al., 2011). The construction of a rheological profile requires the knowledge of several parameters, like strain rate and tectonic style, which are not generally available. Here we tried to understand the rheology of the lithosphere by considering its seismicity and strength deduced from yield stress envelopes versus depth.

The rheological properties of the crust can be roughly quantified using the scheme proposed by Panza and Raykova (2008), i.e., considering the earthquake hypocentres (N) and the seismic energy released (E). As a proxy for the rheology, lack of seismicity does not necessarily imply that the lithosphere is locally more rigid, since the rigid crust is not a sufficient condition for weak seismicity: it may indicate, for example, that there is no active tectonics or that the strain rate is locally lower than that in the surroundings (e.g. Panza and Raykova, 2008; Brandmayr et al., 2011; Wu and Zhang, 2012; Deng et al., 2013; Zhang et al., 2013b).

The yield strength envelope (YSE) is another method that has been widely employed to constrain the rheology of the lithosphere in various tectonic environments (e.g. Ranalli and Murphy, 1987; Wang, 2001; Zang et al., 2005; Pauselli et al., 2010; Muto, 2011; Zhang et al., 2013b). The lithosphere is the uppermost rigid portion of the Earth and its rheological structure can be divided into an upper regime (in which deformation is always brittle), a lower regime (in which deformation is often ductile), and the brittle-ductile transition between them. The corresponding equations and parameters for the regimes have been clearly illustrated by previous studies (Zhang et al., 2013b; Chen et al., 2014).

The upper crust is mostly composed of wet quartzite and the principal component in lithospheric mantle is olivine, while it is hard to determine the rock type in the lower crust, notwithstanding several laboratory measurements (e.g. Kohlstedt et al., 1995). To broaden the menu, we assume that the lower crust is composed of two possible rock groups: the "undried granulite" and the "dry diabase", as proposed by Burov and Watts (2006). In order to evaluate the distribution of the rheological structure of the different tectonic units in the study region, we choose several lithosphere columns (see Figure 5) within these tectonic blocks to calculate the rheological YSEs. The values of the parameters used in the calculation are listed in Table 1.

As for the thickness of the crustal layers, we refer to the crustal structure shown in Figure 2. Geothermal curves are calculated by solving the 1D steady state heat conduction equation using the constraint of the heat flow data provided by Tao and Shen (2008). We adopted the functional form proposed by Lachenbruch (1970) for heat production, which should decrease exponentially with depth, and all the parameters adopted for the geotherms calculation are listed in Table 2.

There are essentially two competing rheological models for the long-term strength of continental lithosphere (Jackson, 2002a, 2002b; Burov and Watts, 2006; Burov, 2011): the dubbed jelly sandwich (JS) model, suggesting that continental lithosphere consists of a weak lower crust sandwiched between a relatively strong upper crust and a strong upper mantle (Chen and Molnar, 1983), and the crème brulee (CB) model, suggesting that the strength of continental lithosphere

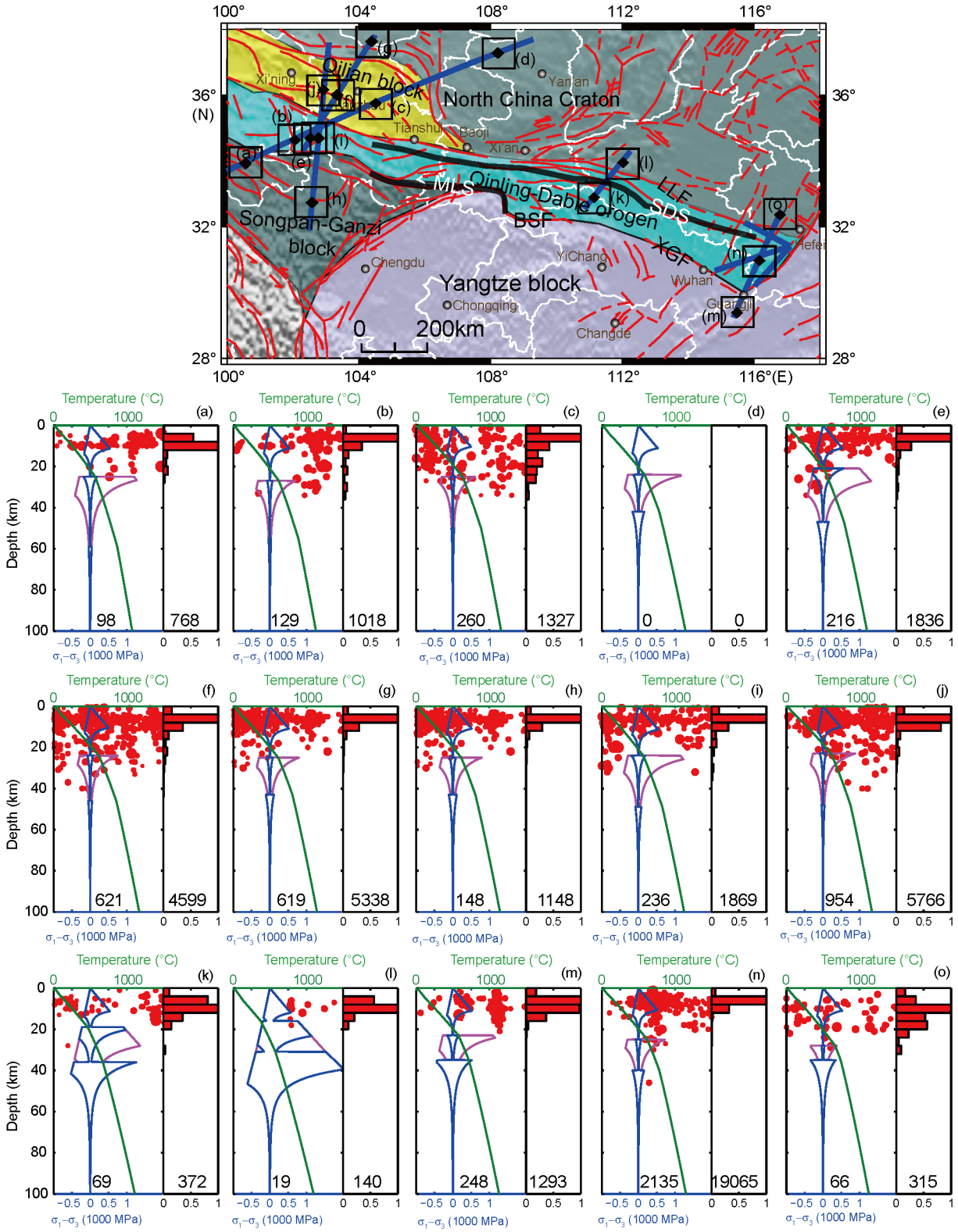

Figure 5 Upper panel: reference positions of (a)–(o). The yield envelope strength, geothermal curve (green lines), seismicity within one degree column (one longitude degree by one latitude degree) (red circles, the seismic events ($M_L \geq 1$) occurred between January 1980 and 2012 edited by Catalogue of the China Earthquake Network Centre (CENC)) and energy release beneath the nine points. The blue lines indicate that the lower crust is assumed to be composed of undried granulite; the purple lines indicate that the lower crust is assumed to be composed of dry diabase. The number in every left panel indicates the earthquake number in one degree column, the number in every right panel indicates the maximum of each histogram when the earthquakes are sorted in depth intervals of 4 km.

Table 1 Ductility parameters assumed in the model calculations[a)]

	Composition	Pre-exponential stress constant, A (MPa^{-n} s^{-1})	Power law exponent, n	Activation energy, Q (kJ mol^{-1})	Reference
Upper crust	Wet quartzite	1.1×10^{-4}	4.0	223	Burov and Watts, 2006
Lower crust	Undried granulite	1.4×10^{4}	4.2	445	Burov and Watts, 2006
	Dry diabase	8	4.7	485	
Lithosphere mantle	Dry olivine	4.85×10^{4}	3.5	535	Burov and Watts, 2006

a) ε is 10^{-14}; surface temperature 10°C; the thickness of upper and lower crust are taken from Figure 2; density of upper crust, lower crust and mantle is 2.7, 2.9, 3.3 g/cm^3, respectively.

Table 2 Parameters used in geothermal calculations[a)]

	H_{sd} (km)	H_{uc} (km)	H_{ct} (km)	k_{sd} (W (m K)$^{-1}$)	A_0 (μW m^{-3})	D (km)	HF (mW m^{-2})	Location (longitude, latitude)
(a)	3	22	59	2.5	2.8	15	60	100.57°E, 33.97°N
(b)	3	24	55	2.5	2.7	15	60	102.07°E, 34.69°N
(c)	3	22	50	2.5	3	15	65	104.53°E, 35.80°N
(d)	4	20	42	2.5	2.6	15	61	108.23°E, 37.32°N
(e)	3	18	47	2.5	2.6	15	60	102.54°E, 34.75°N
(f)	4	20	46	2.5	3	15	66	103.34°E, 36.05°N
(g)	4	21	43	2.5	2.8	15	63	104.39°E, 37.67°N
(h)	4	18	50	2.5	2.4	15	57	102.58°E, 32.81°N
(i)	4	20	49	2.5	2.6	15	60	102.77°E, 34.75°N
(j)	3	20	48	2.5	3.1	15	67	102.91°E, 36.21°N
(k)	3	16	36	2.5	2.3	15	58	111.17°E, 32.97°N
(l)	6	10	31	2.5	2.1	15	57	112.05°E, 34.01°N
(m)	5	18	35	2.5	2.8	15	64	115.51°E, 29.48°N
(n)	3	22	40	2.5	2.7	15	62	116.20°E, 31.06°N
(o)	3	25	35	2.5	2.7	15	61	116.82°E, 32.44°N

a) H_{sd}, H_{uc} and H_{ct} denote the thickness of sediment, upper crust and whole crust, respectively; k_{sd} is the thermal conductivity of sediments; A_0 is the heat production at surface; D is the characteristic depth of heat production; and HF is the surface heat flow, derived from Tao and Shen (2008).

resides entirely in the crust and that the upper mantle is significantly weaker, due to high temperature and weakening by water (Jackson, 2002a, 2002b; Jackson et al., 2008). Supposing the lower crust is composed of granulite, we get the YSEs shown in Figure 5 (blue lines). Yangtze block, North China Craton, Songpan-Ganzi block and Qinling-Dabie orogen present different rheological features, as well as the interior of the Qinling-Dabie orogen. In the western Qinling-Dabie (panels b, e and i, in Figure 5) the lithospheric mantle is weak, while in the central (panel k) and eastern (panel n) Qinling-Dabie the lithospheric mantle is relatively stronger. Songpan-Ganzi block (panels a and h), Qilian block (panels c, f and j) and western Qinling-Dabie are typical examples of the CB model: their strength is high in the upper part and low in the lower part. In comparison with the western part, Yangtze block (panel m), North China Craton (panels d, l and o), the central (panel k) and eastern (panel n) Qinling-Dabie show a stronger lithosphere. Thus, they shall be associated to the JS model, even though the eastern (panel n) Qinling-Dabie has the lowest strength among the six panels.

Supposing the lower crust is composed of dry diabase, the strength in the lower crust (purple lines in Figure 5) becomes higher than in the undried granulite model. However, the rheological classification doesn't change, since the Songpan-Ganzi block, Qilian block western and central Qinling-Dabie orogen also fall into the CB model, even if they have a relatively strong lower crust. The Yangtze block, North China Craton and eastern Qinling-Dabie orogen have strong lower crust and lithospheric mantle; thus, they still belong to the JS model.

No matter what rock is chosen in the lower crust, the western part of the region under our analysis falls into the CB group of lithospheric models, which is consistent with the weak lower crust, and/or continental arc feature (Zhang et al., 2013a), while the eastern part falls into the JS group of lithospheric models (Zhang et al., 2013b). All earthquakes are located in the crust, and the maximum energy released lies at a depth of ~10 km. Notably, few earthquakes occurred at a depth of over 30 km, which is in good agreement with the brittle-ductile transition (BDT) depths of the rheological pro-

file. Specifically, earthquakes mainly occur in the upper crust beneath panel a, while earthquakes in panels b and c locate in the upper and middle crust, respectively. The absence of earthquakes in Ordos basin (panel d) seems to correlate well with the stable and rigid craton. In panels e, f, g, h, i the distribution of earthquakes is quite similar. In the central and eastern part of the region (panels k, l, m, o) earthquakes are relatively less present than in the western part, except panel n, that is characterized by active seismicity with the highest seismic energy release, corresponding to the southernmost part of the Tanlu fault (Deng et al., 2013). The penetration of fluids leads to a decrease of the effective normal stress across the fault planes, which favours the earthquakes generation.

In conclusion, the lithospheric strength implies the degree of stiffness or weakness of the lithosphere, and the seismicity reflects the stress tolerance of rocks and tectonic stress. The stiff region shows weak deformation, corresponding to stable environment and low seismicity areas (if there are no active faults), such as South China and Ordos basin (North China Craton). The weak region shows the possible strong deformation, corresponding to the high seismicity (if there are accumulated forces), such as the margin of Tibet and western Qinling-Dabie. Though the eastern Qinling-Dabie belongs to the JS model, it has the lowest strength among the blocks belonging to the JS model.

5. Seismic velocities of UHP regions

Recognition of UHP metamorphic rocks (i.e. coesite, diamond and other UHP metamorphic minerals) and deep subduction has been one of the most important progresses in the studies of continental dynamics (e.g. Zheng, 2008). Following the traditional description of the plate tectonics theory, the continental crust has a lower density than that of the oceanic crust, thus, is not able to subdue into the relatively high-density mantle. Objections to the original formulation of the continental drift and plate tectonics have been brought on the driving mechanism and on the evidence that subduction occurred to the less dense continental lithosphere in continent-continent collision zones (Pfiffner et al., 1997; Panza et al., 2003; Anderson, 2007; Chen et al., 2014). These evidences and the discovery of coesite, an UHP index mineral in metamorphic supracrustal rocks in Western Alps and Western Norway (Liou et al., 2004), add further challenge to the original formulation of plate tectonics (Doglioni and Panza, 2015). In fact, they demonstrate that the oceanic/continental crust was subducted to a depth of at least 80 km before returning to surface according to the *P-T-t* path (pressure, temperature and time) of the subducted mineral.

Up to now, the UP/UHP rocks have been reported in several terranes worldwide, including the Qinling-Dabie orogen (Zheng et al., 2007; Zheng, 2008), Sulu orogen (Zhang et al., 2005; Frezzotti et al., 2007), North Qilian orogen (Zhang et al., 2007), North Qaidam (Song et al., 2003; Zhang et al., 2009), Altyn (Liu et al., 2012), Western Tianshan in western China (Zhang et al., 2002), Himalayan orogen (Liou et al., 2004), Maksyutov in Russia (Beane et al., 1995; Leech and Ernst, 1998) (Low temperature diamond), Western Gneiss Region in Norway (Hacker et al., 2010), Dora Maira in Italy (Castelli et al., 2007), Zermatt-Saas Fee in Switzerland (Angiboust et al., 2009), Kokchetav in Kazakhstan (de Corte et al., 2000), the Saxonian Erzgebirge in Germany (Willner et al., 2000), Mali in Africa (Jahn et al., 2001), Central Indonesia UHP terrane (Parkinson, 2000), French Massif Central (Lardeaux et al., 2001), Northeast Greenland Caledonides (Gilotti and Ravna, 2002), Neoproterozoic nappes in Southeast Brazil (da Costa Campos Neto and Caby, 2000), Chuacus Complex in northern-central Guatemala (Ortega-Gutiérrez et al., 2004), and Lanterman Range in Antarctica (Ghiribelli et al., 2002).

In order to discuss the seismic velocity and deep subduction models, we considered the 8 terranes in the regions that have been intensively studied with DSS profiles, as shown in Figure 6.

Christensen and Mooney (1995) summarized the results from the DSS profiles available worldwide, and they showed that the thickness and velocity structure of the crust are well correlated with the different tectonic province and they are proof of the processes that have formed and modified the crust. As shown in Figure 6, the global average velocity varies between 5.8–6.3 km/s in the upper crust, 6.3–6.7 km/s in the middle crust and 6.7–7.0 km/s in the lower crust. Since the active seismic results do not supply ranges for subMoho velocities, it must be kept in mind that the values are affected by an uncertainty of ~10%; that is why they are not shown as colour scaled in Figure 6.

Compared with the global velocity model, the velocities in the lower crust are higher than 7.0 km/s beneath Dora Maira (Lardeaux et al., 2006; Boncio et al., 2007), Maksyutov (Stadtlander et al., 1999), Western gneiss region (Stratford et al., 2009), and Sulu (Li, 1991; Bai et al., 2007), whereas the velocities in the uppermost mantle are higher than 8.1 km/s beneath Zematt-Saas Fee (Thouvenot and Perrier, 1980; Ye et al., 1995) and northern Qaidam (Cui et al., 1995). This fact could be explained by the presence of HP/UHP metamorphic rocks (Liu et al., 2003; Luo et al., 2012). The relatively low velocities (not higher than 7.0 km/s) in the lower crust beneath northern Qilian can be explained either by the low resolution of DSS data or by the presence of partial melting (e.g. Hacker et al., 2014). Beneath the Dabie, the upper crust is characterized by a relatively higher velocity, which may indicate that the middle and lower-crust metamorphic rocks are exposed at the surface (Liu et al., 2003; Luo et al., 2012) or the reflection of mountain feature (Ouyang et al., 2014). The

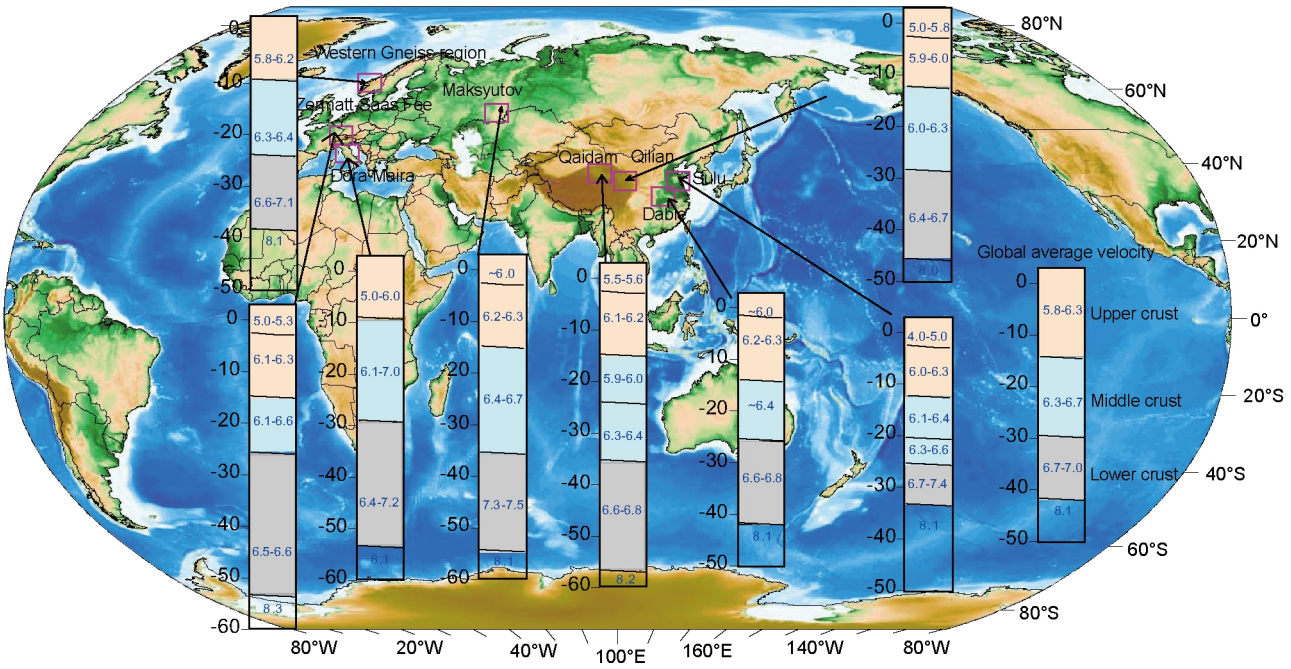

Figure 6 Distribution of typical HP/UHP terranes in the world and variation ranges of their respective average P-wave velocities: Dora Maira (Lardeaux et al., 2006; Thouvenot et al., 2007), Zermatt-Saas Fee (Ye et al., 1995), Maksyutov (Stadtlander et al., 1999), Sulu (Li, 1991; Bai et al., 2007), Dabie (Liu et al., 2003), North Qilian (Zhang et al., 2013a), North Qaidam (Cui et al., 1995), Western Gneiss region (Stratford et al., 2009). Sub-Moho velocities, due to the limited resolving power of available data, are only indicative and may vary in a range of 5% or more; therefore, they are not colour scaled.

absence of the high velocities of lower crust beneath Dabie orogen remains consistent with lithospheric delamination (Gao et al., 1999), high temperature and/or partial melting.

6. Conclusions

Based on the DSS profiles and seismic tomography conducted in the Qinling-Dabie and neighbouring regions, we have made a comparison of the crustal/lithospheric features such as delineated along east-west and north-south sections drawn within the study region. We have then employed seismicity and rheological strength profiles to depict the lithospheric rheological characteristics of these regions. Finally, considering the P-wave velocity, a worldwide comparison was made among typical HP/UHP terranes. Our main conclusions can be summarized as follows:

(1) The different blocks are characterized by their individual seismic velocities. The contrast in seismic velocities between the western and eastern parts indicates the different origin and deformation history.

(2) The rigid blocks, such as South China and Ordos basin (North China Craton), resist deformation and show low seismicity. The weak regions, such as the margin of Tibet and western Qinling-Dabie, experience strong deformation and accumulated stress, thus show active seismicity.

(3) In most of the HP/UHP terranes worldwide, the P-wave velocities in the lower crust are relatively higher than that in the surroundings, whereas the Dabie orogen has a distinctively low-velocity lower crust and lithospheric mantle. This, together with its weak rheological strength, suggests that the lower portion of the lithosphere under the Dabie orogen was likely removed through delamination.

Acknowledgements *The paper is dedicated to the memory of Professor Zhang Zhongjie (1964–2013), who proposed the initial idea of this manuscript. Constructive comments from three anonymous reviewers have greatly improved the manuscript. We thank Dr. Qiu Zhong for valuable discussions and suggestions. We gratefully acknowledge the support offered by the Strategic Priority Research Program (B) of the Chinese Academy of Sciences (Grant No. XDB18030101), the National Natural Science Foundation of China (Grant No. 41504069) and the Italian Projects PRIN 2010–2011, PRIN 2015.*

References

Anderson D L. 2007. Slabs on command—Is there convincing tomographic evidence for whole mantle convection? www.mantleplumes.org/TomographyProblems.html

Angiboust S, Agard P, Jolivet L, Beyssac O. 2009. The Zermatt-Saas ophiolite: The largest (60-km wide) and deepest (*c.* 70–80 km) continuous slice of oceanic lithosphere detached from a subduction zone? Terra Nova, 21: 171–180

Bai Z M, Zhang Z J, Wang Y H. 2007. Crustal structure across the Dabie-Sulu orogenic belt revealed by seismic velocity profiles. J Geophys Eng, 4: 436–442

Bao X, Song X, Xu M, Wang L, Sun X, Mi N, Yu D, Li H. 2013. Crust and upper mantle structure of the North China Craton and the NE Tibetan Plateau and its tectonic implications. Earth Planet Sci Lett, 369-370:

129–137
Beane R J, Liou J G, Coleman R G, Leech M L. 1995. Petrology and retrograde *P-T* path for eclogites of the Maksyutov complex, Southern Ural Mountains, Russia. Isl Arc, 4: 254–266
Boncio P, Mancini T, Lavecchia G, Selvaggi G. 2007. Seismotectonics of strike-slip earthquakes within the deep crust of southern Italy: Geometry, kinematics, stress field and crustal rheology of the Potenza 1990–1991 seismic sequences (M_{max} 5.7). Tectonophysics, 445: 281–300
Brandmayr E, Marson I, Romanelli F, Panza G F. 2011. Lithosphere density model in Italy: No hint for slab pull. Terra Nova, 23: 292–299
Burov E, Watts A. 2006. The long-term strength of continental lithosphere: "Jelly sandwich" or "crème brûlée"? GSA Today, 16: 4
Burov E B. 2011. Rheology and strength of the lithosphere. Mar Pet Geol, 28: 1402–1443
Cao J M, Zhu J S, Wu D C. 1994. Velocity structure of the crust in eastern Qinlinmountain (in Chinese with English abstract). J Chengdu Inst Technol, 21: 11–17
Castelli D, Rolfo F, Groppo C, Compagnoni R. 2007. Impure marbles from the UHP Brossasco-Isasca Unit (Dora-Maira Massif, western Alps): Evidence for Alpine equilibration in the diamond stability field and evaluation of the X(CO_2) fluid evolution. J Metamorph Geol, 25: 587–603
Chen L, Berntsson F, Zhang Z, Wang P, Wu J, Xu T. 2014. Seismically constrained thermo-rheological structure of the eastern Tibetan margin: Implication for lithospheric delamination. Tectonophysics, 627: 122–134
Chen L, Gerya T V. 2016. The role of lateral lithospheric strength heterogeneities in orogenic plateau growth: Insights from 3-D thermo-mechanical modeling. J Geophys Res Solid Earth, 121: 3118–3138
Chen W P, Molnar P. 1983. Focal depths of intracontinental and intraplate earthquakes and their implications for the thermal and mechanical properties of the lithosphere. J Geophys Res, 88: 4183–4214
Christensen N I, Mooney W D. 1995. Seismic velocity structure and composition of the continental crust: A global view. J Geophys Res, 100: 9761–9788
de Corte K, Korsakov A, Taylor W R, Cartigny P, Ader M, De Paepe P. 2000. Diamond growth during ultrahigh-pressure metamorphism of the Kokchetav massif, northern Kazakhstan. Isl Arc, 9: 428–438
Cui Z Z, Li Q S, Wu C D, Yin Z X, Liu H B. 1995. The crustal structure and deeptectonics along Golmud-Ejinaqi transect (in Chinese with English abstract). Chin J Geophys, 38(Suppl II): 15–28
da Costa Campos Neto M, Caby R. 2000. Terrane accretion and upward extrusion of high-pressure granulites in the Neoproterozoic nappes of southeast Brazil: Petrologic and structural constraints. Tectonics, 19: 669–687
Deng Y, Li S, Fan W L, Liu J. 2011. Crustal structure beneath South China revealed by deep seismic soundings and its dynamics implications (in Chinese with English abstract). Chin J Geophys, 54: 2560–2574
Deng Y, Fan W, Zhang Z, Badal J. 2013. Geophysical evidence on segmentation of the Tancheng-Lujiang fault and its implications on the lithosphere evolution in East China. J Asian Earth Sci, 78: 263–276
Doglioni C, Panza G. 2015. Chapter One-Polarized plate tectonics. Adv Geophys, 56: 1–167
Dong S W, Wu X Z, Gao R, Lu D Y, Li Y K, He Y Q, Tang J F, Cao F Y, Hou M J, Huang D J. 1998. On the crust velocity levels and dynamics of the Dabieshan orogenic belt (in Chinese with English abstract). Chin J Geophys, 41: 349–361
Dong S W, Li Q S, Gao R, Liu F T, Xu P F, Liu X C, Xue H M, Guan Y. 2008. Moho-mapping in the Dabie ultrahigh-pressure collisional orogen, central China. Am J Sci, 308: 517–528
Dong Y, Zhang G, Neubauer F, Liu X, Genser J, Hauzenberger C. 2011. Tectonic evolution of the Qinling orogen, China: Review and synthesis. J Asian Earth Sci, 41: 213–237
Frezzotti M L, Ferrando S, Dallai L, Compagnoni R. 2007. Intermediate Alkali-Alumino-silicate aqueous solutions released by deeply subducted continental crust: Fluid evolution in UHP OH-rich Topaz-Kyanite quartzites from Donghai (Sulu, China). J Petrol, 48: 1219–1241
Gao S, Zhang B, Jin Z, Kern H. 1999. Lower crustal delamination in the Qinling-Dabie orogenic belt. Sci China Ser D-Earth Sci, 42: 423–433
Ghiribelli B, Frezzotti M L, Palmeri R. 2002. Coesite in eclogites of the Lanterman Range (Antarctica): Evidence from textural and Raman studies. Eur J Mineral, 14: 355–360
Gilotti J A, Ravna E J K. 2002. First evidence for ultrahigh-pressure metamorphism in the North-East Greenland Caledonides. Geology, 30: 551–554
Hacker B R, Andersen T B, Johnston S, Kylander-Clark A R C, Peterman E M, Walsh E O, Young D. 2010. High-temperature deformation during continental-margin subduction & exhumation: The ultrahigh-pressure Western Gneiss Region of Norway. Tectonophysics, 480: 149–171
Hacker B R, Ritzwoller M H, Xie J. 2014. Partially melted, mica-bearing crust in Central Tibet. Tectonics, 33: 1408–1424
Jackson J. 2002a. Faulting, flow, and the strength of the continental lithosphere. Int Geol Rev, 44: 39–61
Jackson J. 2002b. Strength of the continental lithosphere: Time to abandon the jelly sandwich? GSA Today, 12: 4–9
Jackson J, McKenzie D, Priestley K, Emmerson B. 2008. New views on the structure and rheology of the lithosphere. J Geol Soc, 165: 453–465
Jahn B, Caby R, Monie P. 2001. The oldest UHP eclogites of the World: Age of UHP metamorphism, nature of protoliths and tectonic implications. Chem Geol, 178: 143–158
Jiang C, Yang Y, Zheng Y. 2016. Crustal structure in the junction of Qinling Orogen, Yangtze craton and Tibetan Plateau: Implications for the formation of the Dabashan Orocline and the growth of Tibetan Plateau. Geophys J Int, 205: 1670–1681
Jiang G, Zhang G, Lü Q, Shi D, Xu Y. 2013. 3-D velocity model beneath the Middle-Lower Yangtze River and its implication to the deep geodynamics. Tectonophysics, 606: 36–47
Kohlstedt D L, Evans B, Mackwell S J. 1995. Strength of the lithosphere: Constraints imposed by laboratory experiments. J Geophys Res, 100: 17587–17602
Lachenbruch A H. 1970. Crustal temperature and heat production: Implications of the linear heat-flow relation. J Geophys Res, 75: 3291–3300
Lardeaux J M, Ledru P, Daniel I, Duchene S. 2001. The Variscan French Massif Central—A new addition to the ultra-high pressure metamorphic "club": Exhumation processes and geodynamic consequences. Tectonophysics, 332: 143–167
Lardeaux J M, Schwartz S, Tricart P, Paul A, Guillot S, Béthoux N, Masson F. 2006. A crustal-scale cross-section of the south-western Alps combining geophysical and geological imagery. Terra Nova, 18: 412–422
Leech M L, Ernst W G. 1998. Graphite pseudomorphs after diamond? A carbon isotope and spectroscopic study of graphite cuboids from the Maksyutov Complex, south Ural Mountains, Russia. Geochim Cosmochim Acta, 62: 2143–2154
Li T S. 1991. Features of gravitational and magnetic anomalies and crustal structurealong the Lianyungang-Linyi-Sishui profile (in Chinese with English abstract). J Seismol Res, 14:141–146
Liou J G, Tsujimori T, Zhang R Y, Katayama I, Maruyama S. 2004. Global UHP metamorphism and continental subduction/collision: The Himalayan Model. Int Geol Rev, 46: 1–27
Liou J G, Zhang R Y, Jahn B M. 2000. Petrological and geochemical characteristics of ultrahigh-pressure metamorphic rocks from the Dabie-Sulu Terrane, East-Central China. Int Geol Rev, 42: 328–352
Liu F T, Xu P F, Liu J S, Yin Z X, Qin J Y, Zhang X K, Zhang C K, Zhao J R. 2003. Thecrustal velocity structure of the continental deep subduction belt: Study on theeastern Dabie orogen by seismic wide-angle reflection/refraction (in Chinese with English abstract). Chin J Geophys, 46: 366–372
Liu L, Wang C, Cao Y T, Chen D L, Kang L, Yang W Q, Zhu X H. 2012. Geochronology of multi-stage metamorphic events: Constraints on episodic zircon growth from the UHP eclogite in the South Altyn, NW

China. Lithos, 136-139: 10–26
Liu M, Mooney W D, Li S, Okaya N, Detweiler S. 2006. Crustal structure of the northeastern margin of the Tibetan plateau from the Songpan-Ganzi terrane to the Ordos basin. Tectonophysics, 420: 253–266
Luo Y, Xu Y, Yang Y. 2012. Crustal structure beneath the Dabie orogenic belt from ambient noise tomography. Earth Planet Sci Lett, 313-314: 12–22
Meng Q R, Zhang G W. 2000. Geologic framework and tectonic evolution of the Qinling orogen, central China. Tectonophysics, 323: 183–196
Muto J. 2011. Rheological structure of northeastern Japan lithosphere based on geophysical observations and rock mechanics. Tectonophysics, 503: 201–206
Ortega-Gutiérrez F, Solari L A, Solé J, Martens U, Gómez-Tuena A, Morán-Ical S, Reyes-Salas M. 2004. Polyphase, high-temperature eclogite-facies metamorphism in the Chuacús Complex, central Guatemala: Petrology, geochronology, and tectonic implications. Int Geol Rev, 46: 445–470
Ouyang L, Li H, Lü Q, Yang Y, Li X, Jiang G, Zhang G, Shi D, Zheng D, Sun S, Tan J, Zhou M. 2014. Crustal and uppermost mantle velocity structure and its relationship with the formation of ore districts in the Middle-Lower Yangtze River region. Earth Planet Sci Lett, 408: 378–389
Pan S, Niu F. 2011. Large contrasts in crustal structure and composition between the Ordos plateau and the NE Tibetan Plateau from receiver function analysis. Earth Planet Sci Lett, 303: 291–298
Panza G F, Pontevivo A, Chimera G, Raykova R, Aoudia A. 2003. The lithosphere-asthenosphere: Italy and surroundings. Episodes, 26: 169–174
Panza G F, Raykova R B. 2008. Structure and rheology of lithosphere in Italy and surrounding. Terra Nova, 20: 194–199
Parkinson C D. 2000. Coesite inclusions and prograde compositional zonation of garnet in whiteschist of the HP-UHPM Kokchetav massif, Kazakhstan: A record of progressive UHP metamorphism. Lithos, 52: 215–233
Pauselli C, Ranalli G, Federico C. 2010. Rheology of the Northern Apennines: Lateral variations of lithospheric strength. Tectonophysics, 484: 27–35
Pfiffner O A, Lehner P, Heitzmann P, Müller St, Steck A. 1997. Deep Structure of the Swiss Alps, Results of NRP 20. Basel: Birkhauser Verlag. 380
Ranalli G, Murphy D C. 1987. Rheological stratification of the lithosphere. Tectonophysics, 132: 281–295
Rudnick R L, Fountain D M. 1995. Nature and composition of the continental crust: A lower crustal perspective. Rev Geophys, 33: 267–309
Shen W, Ritzwoller M H, Schulte-Pelkum V, Lin F C. 2013. Joint inversion of surface wave dispersion and receiver functions: A Bayesian Monte-Carlo approach. Geophys J Int, 192: 807–836
Shen W, Ritzwoller M H, Kang D, Kim Y H, Lin F C, Ning J, Wang W, Zheng Y, Zhou L. 2016. A seismic reference model for the crust and uppermost mantle beneath China from surface wave dispersion. Geophys J Int, 206: 954–979
Song S G, Yang J S, Xu Z Q, Liou J G, Shi R D. 2003. Metamorphic evolution of the coesite-bearing ultrahigh-pressure terrane in the North Qaidam, Northern Tibet, NW China. J Metamorph Geol, 21: 631–644
Stadtlander R, Mechie J, Schulze A. 1999. Deep structure of the southern Ural mountains as derived fromwide-angle seismic data. Geophys J Int, 137: 501–515
Stratford W, Thybo H, Faleide J I, Olesen O, Tryggvason A. 2009. New Moho Map for onshore southern Norway. Geophys J Int, 178: 1755–1765
Tao W, Shen Z. 2008. Heat flow distribution in Chinese continent and its adjacent areas. Prog Nat Sci, 18: 843–849
Thouvenot F, Perrier G. 1980. Seismic evidence of a crustal overthrust in the Western Alps. Pure Appl Geophys, 119: 163–184
Thouvenot F, Paul A, Fréchet J, Béthoux N, Jenatton L, Guiguet R. 2007. Are there really superposed Mohos in the southwestern Alps? New seismic data from fan-profiling reflections. Geophys J Int, 170: 1180–1194
Vanderhaeghe O, Teyssier C. 2001. Crustal-scale rheological transitions during late-orogenic collapse. Tectonophysics, 335: 211–228
Wang Q, Ji S, Salisbury M H, Xia B, Pan M, Xu Z. 2005. Shear wave properties and Poisson's ratios of ultrahigh-pressure metamorphic rocks from the Dabie-Sulu orogenic belt, China: Implications for crustal composition. J Geophys Res, 110: B08208
Wang Q, Wyman D A, Xu J, Jian P, Zhao Z, Li C, Xu W, Ma J, He B. 2007. Early Cretaceous adakitic granites in the Northern Dabie Complex, central China: Implications for partial melting and delamination of thickened lower crust. Geochim Cosmochim Acta, 71: 2609–2636
Wang Y. 2001. Heat flow pattern and lateral variations of lithosphere strength in China mainland: Constraints on active deformation. Phys Earth Planet Inter, 126: 121–146
Willner A P, Krohe A, Maresch W V. 2000. Interrelated P-T-t-d paths in the variscan erzgebirge dome (Saxony, Germany): Constraints on the rapid exhumation of high-pressure rocks from the root zone of a collisional orogen. Int Geol Rev, 42: 64–85
Wu J, Zhang Z. 2012. Spatial distribution of seismic layer, crustal thickness, and Vp/Vs ratio in the Permian Emeishan Mantle Plume region. Gondwana Res, 22: 127–139
Wu Y B, Zheng Y F. 2013. Tectonic evolution of a composite collision orogen: An overview on the Qinling-Tongbai-Hong'an-Dabie-Sulu orogenic belt in central China. Gondwana Res, 23: 1402–1428
Xie J, Ritzwoller M H, Shen W, Yang Y, Zheng Y, Zhou L. 2013. Crustal radial anisotropy across Eastern Tibet and the Western Yangtze Craton. J Geophys Res-Solid Earth, 118: 4226–4252
Xu T, Zhang Z J, Tian X B, Liu B F, Bai Z M, Lu Q T, Teng J W. 2014. Crustal structure beneath the Middle-Lower Yangtze metallogenic belt and its surrounding areas: Constraints from active source seismic experiment along the Lixin to Yixing profile in East China. Acta Petrol Sin, 30: 918–930
Ye S, Ansorge J, Kissling E, Mueller S. 1995. Crustal structure beneath the eastern Swiss Alps derived from seismic refraction data. Tectonophysics, 242: 199–221
Zang S X, Qiang Wei R, Liu Y G. 2005. Three-dimensional rheological structure of the lithosphere in the Ordos block and its adjacent area. Geophys J Int, 163: 339–356
Zhang G W, Dong Y B, Lai S C, Guo A L, Meng Q R, Liu S F, Cheng S Y, Yao A P, Zhang Z Q, Pei X Z, Li S Z. 2003. Mianlüe tectonic zone and Mianlüe suture zone on southern margin of Qinling-Dabie orogenic belt. Sci China Ser D-Earth Sci, 47: 300–316
Zhang G W, Cheng S, Guo A, Dong Y, Lai S, Yao A. 2004. Mianlue paleosuture on the southern margin of the Central Orogenic System in Qinling-Dabie with a discussion of the assembly of the main part of the continent of China (in Chinese with English abstract). Geol Bull, 23: 846–853
Zhang G, Zhang L, Song S, Niu Y. 2009. UHP metamorphic evolution and SHRIMP geochronology of a coesite-bearing meta-ophiolitic gabbro in the North Qaidam, NW China. J Asian Earth Sci, 35: 310–322
Zhang J, Ma C, Li J, Pan Y. 2015. Petrogenesis of Early Cretaceous alkaline dolerite dykes in the Dabie Orogen, China: Constraints on the timing of lithospheric thinning. Lithos, 216-217: 17–30
Zhang J X, Meng F C, Wan Y S. 2007. A cold Early Palaeozoic subduction zone in the North Qilian Mountains, NW China: Petrological and U-Pb geochronological constraints. J Metamorph Geol, 25: 285–304
Zhang L, Ellis D J, Williams S, Jiang W. 2002. Ultra-high pressure metamorphism in western Tianshan, China: Part II. Evidence from magnesite in eclogite. Am Miner, 87: 861–866
Zhang X K, Jia S X, Zhao J R, Zhang C K, Yang J, Wang F Y, Zhang J S, Liu B F, Sun G W, Pan S Z. 2008. Crustal structures beneath West Qinling-East Kunlun orogen and its adjacent area—Results of wide-angle seismic reflection and refractionexperiment (in Chinese with English abstract). Chin J Geophys, 51: 439–450
Zhang X M, Teng J, Sun R, Romanelli F, Zhang Z, Panza G F. 2014. Struc-

tural model of the lithosphere-asthenosphere system beneath the Qinghai-Tibet Plateau and its adjacent areas. Tectonophysics, 634: 208–226

Zhang Z, Bai Z, Klemperer S L, Tian X, Xu T, Chen Y, Teng J. 2013a. Crustal structure across northeastern Tibet from wide-angle seismic profiling: Constraints on the Caledonian Qilian orogeny and its reactivation. Tectonophysics, 606: 140–159

Zhang Z, Deng Y, Chen L, Wu J, Teng J, Panza G. 2013b. Seismic structure and rheology of the crust under mainland China. Gondwana Res, 23: 1455–1483

Zhang Z, Teng J, Romanelli F, Braitenberg C, Ding Z, Zhang X, Fang L, Zhang S, Wu J, Deng Y, Ma T, Sun R, Panza G F. 2014. Geophysical constraints on the link between cratonization and orogeny: Evidence from the Tibetan Plateau and the North China Craton. Earth-Sci Rev, 130: 1–48

Zhang Z M, Zhang J F, You Z D, Shen K. 2005. Ultrahigh-pressure metamorphic P-T-t path of the Sulu orogenic belt, eastern central China. Acta Petrol Sin, 21: 257–270

Zheng Y F. 2008. A perspective view on ultrahigh-pressure metamorphism and continental collision in the Dabie-Sulu orogenic belt. Chin Sci Bull, 53: 3081–3104

Zheng Y F, Gao T S, Wu Y B, Gong B, Liu X M. 2007. Fluid flow during exhumation of deeply subducted continental crust: Zircon U-Pb age and O-isotope studies of a quartz vein within ultrahigh-pressure eclogite. J Metamorph Geol, 25: 267–283

Zheng Y, Shen W, Zhou L, Yang Y, Xie Z, Ritzwoller M H. 2011. Crust and uppermost mantle beneath the North China craton, northeastern China, and the Sea of Japan from ambient noise tomography. J Geophys Res, 116: B12312

Zheng T, Zhu R, Zhao L, Ai Y. 2012. Intralithospheric mantle structures recorded continental subduction. J Geophys Res, 117: B03308

Zheng T Y, Zhao L, He Y M, Zhu R X. 2014. Seismic imaging of crustal reworking and lithospheric modification in eastern China. Geophys J Int, 196: 656–670

Zhou L, Xie J, Shen W, Zheng Y, Yang Y, Shi H, Ritzwoller M H. 2012. The structure of the crust and uppermost mantle beneath South China from ambient noise and earthquake tomography. Geophys J Int, 189: 1565–1583